Enhancement of drag reduction in particle-laden turbulent flows under span-wise wall oscillation

Jiafeng Xie,[1] Jianxin Hu,[2] Chenlin Zhu,[3,*] Xiaoxuan Kang,[1] and Dingyi Pan[1,†]

[1]*State Key Laboratory of Fluid Power and Mechatronic Systems and Department of Engineering Mechanics, Zhejiang University, Hangzhou 310027, China*

[2]*Key Laboratory of Fluid Transmission Technology of Zhejiang Province, Zhejiang Sci-Tech University, Hangzhou 310018, China*

[3]*Key Laboratory of Intelligent Manufacturing Quality Big Data Tracing and Analysis of Zhejiang Province, China Jiliang University, Hangzhou 310018, China*

(Received 19 June 2025; accepted 2 October 2025; published 16 October 2025)

We report that span-wise sinusoidal wall oscillations can significantly reduce drag in wall-bounded turbulent flows laden with neutrally buoyant, finite-size spherical particles—surpassing the drag reduction observed in corresponding single-phase flows. Direct numerical simulations reveal that this enhanced drag reduction arises from a coupling mechanism between the suspended particles and the wall motion. The span-wise Stokes flow induces particle migration toward the channel center and suppresses near-wall turbulence, thereby reducing the effective viscosity. Quantitatively, we identify an approximately linear relationship linking the coupling-induced drag reduction to both the oscillation-driven variation in near-wall particle volume fraction and the influence of particle size. These findings uncover a previously unrecognized synergistic mechanism for turbulent multiphase drag reduction, bridging Einstein's viscosity model with turbulent boundary layer theory. This insight suggests a approach to actively control wall-bounded multiphase turbulence, with broad implications for fluid mechanics and complex flow systems.

DOI: 10.1103/b81f-6gvc

I. INTRODUCTION

In addition to occurring naturally, wall-bounded suspension flow is widespread in a variety of industrial processes, such as pipeline transportation [1,2], fluidized beds [3], and pharmaceutical processes [4]. The presence of suspended particles can affect wall drag by modulating near-wall turbulent structures [5]. Unlike single-phase turbulence, where control strategies are well established, the physics of turbulence modulation in particle-laden flows remains to be explored. It is widely acknowledged that finite-size particles cause larger wall drag than the single-phase flow. According to Balachandar and Eaton [6], the augmentation of the particle-laden flow's inertia, the rise in dissipation brought on by particle drag, and the increase in the flow's effective viscosity are the three main mechanisms for modulating turbulence in dilute particle-laden suspensions. Despite progress in characterizing such effects, controlling turbulence and reducing drag in particle-laden flows has received little attention, which is critical for sustainable development. This presents a critical opportunity: Can fundamental insights into wall-bounded turbulence enable the control of more complex, multiphase flows?

There are many different drag reduction techniques available today, which can be broadly classified into two groups, i.e., active and passive technologies. While the former involves span-wise wall oscillation [7,8] and stream-wise traveling waves of span-wise wall velocity [9–13], the latter involves modifying the surface geometry to include longitudinal ribs and additional slits [14,15], adding polymer additives [16–19], etc. Significant drag reduction can be accomplished with these strategies. Among these, the high controllability of active drag reduction technology has attracted a lot of interest recently. For the span-wise wall oscillation approach, the significant weakening of stream-wise wall friction is closely associated with a thin, highly sheared Stokes layer formed near the wall by oscillation [20]. The oscillations displace turbulence toward the channel center, producing a thickened viscous sublayer indicative of drag reduction [21]. Fundamentally, drag reduction is primarily due to the enhancement of turbulent dissipation, which suppresses turbulent activity [22]. In general, an enhancement of turbulence dissipation and a corresponding decrease of turbulence production, the hysteresis effect, the properties of the near-wall vortex structures, a reduction of sweep and ejection events, etc., are connected with the regulation of turbulent drag by wall motion [23]. But as of right now, active actuated technology is mostly utilized in single-phase flow—Particle-laden flow has not yet benefited from its application. A key challenge lies in understanding the multiway coupling between wall motions, turbulence, and particle dynamics—including how the span-wise Stokes motion stimulated by wall oscillations alters particle migration and how finite-size particles, in turn, reshape the near-wall turbulence and Stokes layer.

*Contact author: zhuclgary@foxmail.com
†Contact author: dpan@zju.edu.cn

Published by the American Physical Society under the terms of the Creative Commons Attribution 4.0 International license. Further distribution of this work must maintain attribution to the author(s) and the published article's title, journal citation, and DOI.

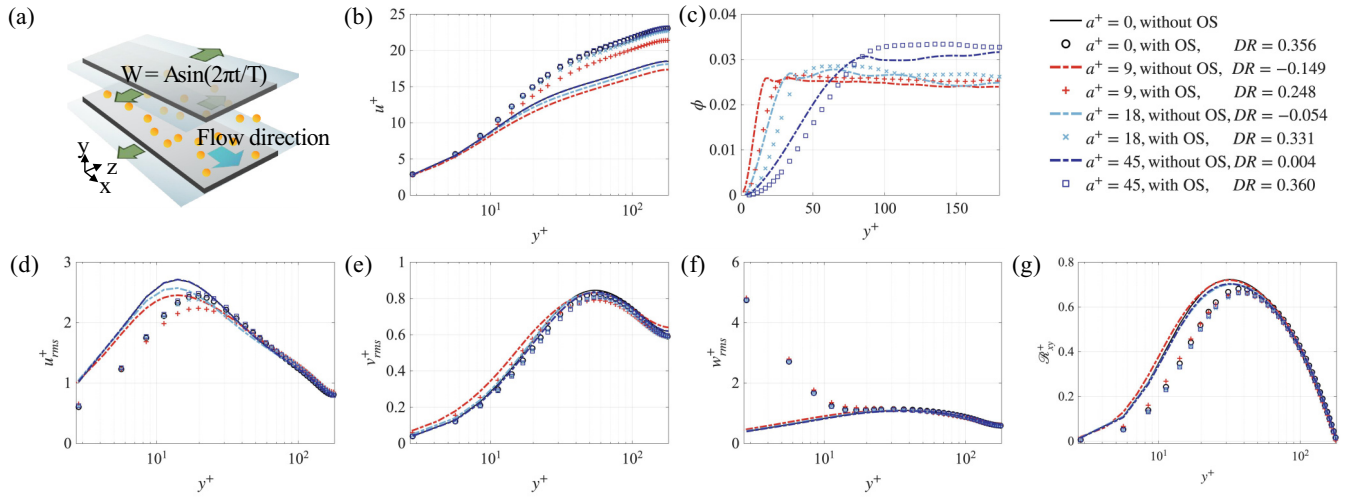


FIG. 1. (a) Schematic diagram of particle-laden turbulent channel flow with span-wise wall oscillations. Effect of span-wise OS with $T^+ = 75$ on (b) stream-wise velocity profiles u^+, (c) particle volume fraction profiles ϕ, (d) stream-wise rms velocity profiles $u^+_{\rm rms}$, (e) wall-normal rms velocity profiles $v^+_{\rm rms}$, (f) span-wise rms velocity profiles $w^+_{\rm rms}$, and (g) Reynolds stress profiles $\mathcal{R}^+_{xy}$.

In the current study, we demonstrate that span-wise wall oscillation—a canonical model of Stokes' second problem—can significantly reduce drag in a fully developed wall-bounded turbulent flow laden with neutrally buoyant finite-size particles. Using fully resolved direct numerical simulations (DNS), we investigate the modulation effect of span-wise wall oscillation on turbulent flows carrying finite-size particles, with particular emphasis on the coupling regimes between wall oscillations and finite-size particles, particularly the boundary layer's dynamics. Our findings reveal fundamental insights into the control of particle-laden turbulence via span-wise oscillatory wall forcing. Thus, the application of span-wise wall oscillation technology in pertinent particle-laden flow scenarios is theoretically and prospectively supported by this study.

II. NUMERICAL METHOD AND SETUPS

In this work, we simulate the wall-bounded turbulent flows laden with finite-size particles under span-wise wall oscillation conditions using the interface-resolved direct-forcing fictitious domain (DF/FD) method [24]. The FD method uses pseudoforce terms to compel the internal fictitious fluids to comply with rigid body motion constraints, based on the assumption that the particle's interior is filled with fluid. The governing Navier-Stokes equation is

$$\partial \mathbf{u}/\partial t + \mathbf{u}\cdot\nabla\mathbf{u} = \nabla^2\mathbf{u}/Re_\tau - \nabla p + \boldsymbol{\lambda} \quad \text{in } \Omega, \tag{1}$$

where $\mathbf{u}$ represents the velocity, p indicates the fluid pressure with the exclusion of the constant pressure gradient, and $\boldsymbol{\lambda}$ is the distributed Lagrange multiplier: It is zero in the fluid region and is distributed over the particle inner domain $P(t)$ for the constraint that all inner fluids move as a rigid body. The friction Reynolds number is defined as $Re_\tau = u_\tau H/\nu_0$, with u_τ the shear velocity, ν_0 the fluid viscosity, and H half of the channel height. The particle motion is governed by

$$\mathbf{u} = \mathbf{U} + \boldsymbol{\omega}_p \times \mathbf{r} \quad \text{in } P(t), \tag{2}$$

$$(\rho_r - 1)V_p^*\left(\frac{\mathrm{d}\mathbf{U}}{\mathrm{dt}} - Fr\frac{\mathbf{g}}{g}\right) = -\int_P \boldsymbol{\lambda}\,\mathrm{d}\mathbf{x}, \tag{3}$$

$$(\rho_r - 1)J^*\frac{\mathrm{d}\boldsymbol{\omega}_p}{\mathrm{dt}} = -\int_P \mathbf{r}\times\boldsymbol{\lambda}\,\mathrm{d}\mathbf{x}, \tag{4}$$

where $\mathbf{U}$ and $\boldsymbol{\omega}_p$ are the translational and angular velocities of the particle, and $\mathbf{r}$ is the position vector relative to the mass center of the particle. Here, $\rho_r = \rho_p/\rho_f$ is the particle-fluid density ratio with ρ_p and ρ_f denoting the particle and fluid densities, $V_p^* = V_p/L_c^3$ the dimensionless particle volume, $J^* = J/(\rho_p L_c^5)$ the dimensionless moment of inertia, $g = |\mathbf{g}|$ the gravitational acceleration, and $Fr = gL_c/u_\tau^2$ the Froude number. Lagrangian points are arranged as homogeneously as possible inside the sphere [25] and all the statistics are retained together with the sphere center information to characterize the solid phase. The particle collisions are described by a repulsive force model that only takes the normal component of the collision into account.

Numerical cases are categorized into single-phase (SP) and particle-laden (PL) flows based on the presence of particles. The SP cases serve as a baseline to highlight the effects of oscillatory actuation, while PL cases elucidate the role of particle dynamics. The computational domain is a cuboid with dimensions of $8H$, $2H$, and $4H$ for directions of stream-wise (x), wall-normal (y), and span-wise (z), as demonstrated in Fig. 1(a). Span-wise oscillation with no-slip wall boundary conditions is applied, and periodic boundary conditions are used in the stream-wise and span-wise directions. In this work, turbulent flows are driven by a constant pressure gradient with a friction Reynolds number of $Re_\tau = 180$. In PL cases, the particle radii are $a/H = 0.05$, 0.075, 0.1, 0.2, 0.25, and 0.3, and the bulk particle volume fraction ϕ_b is 2.36%. The grid resolution is $1024 \times 256 \times 512$ for $a/H = 0.05$ and $a/H = 0.075$, and $512 \times 128 \times 256$ for other cases (including SP cases). In all cases, the characteristic scales are ν_0/u_τ for length, u_τ for velocity, and ν_0/u_τ^2 for time. Parameters marked with superscript "+" are dimensionless,

such as $y^+ = y/(\nu_0/u_\tau)$, $u^+ = u/u_\tau$, and $t^+ = t/(\nu_0/u_\tau^2)$. The dimensionless span-wise oscillation is $W^+ = W/(\nu_0/u_\tau) = A^+ \sin(2\pi t^+/T^+)$, with amplitude $A^+ = 12$ and period $T^+ = 40$–170.

III. RESULTS

Current method has been rigorously validated for particle-laden turbulent flow in our previous works [26,27]. One distinguishing impact of oscillation on PL flow is the modification of the time-averaged stream-wise velocity profile of the fluid phase $u^+(y^+)$ and the particle volume fraction profile $\phi(y^+)$, as shown in Figs. 1(b) and 1(c). It can be clearly observed that, under span-wise wall oscillations, the mean velocity in the bulk region ($y^+ > 10$) is significantly greater than that in all nonoscillatory cases, indicating a higher flow flux and thus a lower flow drag. Particles near the wall migrate toward the channel center due to shear-induced lift [28,29], resulting in a reduction in local particle volume fraction in the vicinity of the wall—It is an inherent property of PL channel flow. In the present oscillatory configuration, the span-wise velocity gradient $\mathrm{d}w^+/\mathrm{d}y^+$ may also induce wall-normal particle displacements within each oscillation cycle. The net effect of this mechanism likely depends on particle size and inertia, which makes it a complex problem worthy of future investigation. More prominently, wall oscillations steepen the near-wall stream-wise velocity gradient $\mathrm{d}u^+/\mathrm{d}y^+$ through span-wise Stokes motion as illustrated in Fig. 1(b), thereby enhancing particle migration toward the channel center [Fig. 1(c)]. In addition, compared to the nonoscillatory PL conditions, drag in the oscillatory flow may also be somewhat decreased by suppressing the formation of the particle layer in the near-wall region [30,31]. Such changes alter the flow structures, especially in the near-wall region, which predominately affects the overall flow drag.

The root mean square (rms) of the fluid velocities (u^+_{rms}, v^+_{rms}, w^+_{rms}) and time-averaged Reynolds stress ($\mathcal{R}^+_{xy} = -\langle u'^+ v'^+ \rangle$) are plotted in Figs. 1(d)–1(g), where u'^+ and v'^+ are fluctuating stream-wise and wall-normal velocities, respectively. In both the nonoscillatory and oscillatory cases, the addition of small and medium particles ($a^+ = 9, 18$) attenuates the peak stream-wise rms velocity while enhancing the wall-normal and span-wise rms velocities near the wall [26,32]. This behavior is mainly attributed to the disruption of near-wall vortical structures by smaller particles. In contrast, large particles ($a^+ = 45$) remain scarce in the near-wall region [Fig. 1(c)] and exert a much weaker influence, yielding velocity profiles close to those of single-phase flow. These trends correspond to higher near-wall $\mathcal{R}^+_{xy}$ (drag increase) for smaller particles and nearly unchanged $\mathcal{R}^+_{xy}$ (no obvious drag variation) for larger particles (shown in the legend), as reported in Ref. [5]. The effect of particle addition on span-wise rms velocity is comparatively minor. Wall oscillations further suppress the near-wall stream-wise and wall-normal rms velocities, thereby reducing Reynolds stress, weakening turbulence activity, and ultimately leading to drag reduction. Notably, the span-wise rms velocity in oscillatory cases is much larger compared with the corresponding nonoscillatory case due to the imposed wall motion, with its magnitude close to the mean absolute wall velocity, $2A^+/\pi$.

The skin friction coefficient is defined as $C_f = 2\tau_w/U^2$, where U is the temporal-spatial-averaged bulk velocity, $\tau_w = \rho_f u_\tau^2$ is the mean wall shear stress, and ρ_f is the fluid density. The shear velocity u_τ is kept constant in our simulations. The bulk velocity in varying cases is shown in Fig. 2(a). U^+ at oscillatory conditions keeps larger than the baseline single-phase nonoscillatory flow, indicating the drag reduction with the span-wise wall forcing. The skin friction coefficient for the baseline single-phase nonoscillatory flow, $C_{f,\mathrm{base}}$, and that under coupled particle-laden flow with span-wise wall oscillation, $C_{f,p+o}$, yield the drag reduction rate DR:

$$\mathrm{DR} = 1 - \frac{C_{f,p+o}}{C_{f,\mathrm{base}}} = 1 - \frac{U^{+2}_{\mathrm{base}}}{U^{+2}_{p+o}}, \tag{5}$$

where $U^+_{\mathrm{base}} = 15.89$ and U^+_{p+o} are the temporal-spatial-averaged dimensionless velocities for the baseline and coupled conditions (with constant driven pressure), respectively. Figure 2(b) shows DR at different T^+ and a^+. For both SP and PL flows, DR first increases and then decreases with the increase of T^+, and the optimal drag reduction is achieved around $T^+ = 80$, which is consistent with previous understandings [8,23,33].

When establishing DR predictions, one must take the impact of near-wall particle migration arising from particle-oscillation coupling into account as shown in Fig. 1(b). Herein, we decompose the overall drag reduction rate DR into three components: drag reduction rate due to span-wise wall oscillation DR_o, particle presence DR_p, and their coupling $\mathrm{DR}_{\mathrm{coup}}$. The first two are defined as

$$\mathrm{DR}_o = 1 - \frac{C_{f,o}}{C_{f,\mathrm{base}}}, \quad \mathrm{DR}_p = 1 - \frac{C_{f,p}}{C_{f,\mathrm{base}}}. \tag{6}$$

Here, $C_{f,o}$ and $C_{f,p}$ denote the skin friction coefficients of the oscillating single-phase flow and the particle-laden flow without wall oscillations, respectively. Based on these definitions, the coupling contribution is obtained as

$$\mathrm{DR}_{\mathrm{coup}} = \mathrm{DR} - (\mathrm{DR}_o + \mathrm{DR}_p). \tag{7}$$

This decomposition is an exact algebraic identity based on the definitions above, rather than an approximation. It provides a convenient framework to assess how the drag reduction induced by wall oscillations and particle presence interact nonlinearly through $\mathrm{DR}_{\mathrm{coup}}$. A similar decomposition strategy has also been adopted in previous studies, e.g., Li *et al.* [34], to identify coupling effects between wall slip boundary and span-wise oscillation. The oscillatory contribution DR_o is predicted using the dimensionless parameter $S^+ = y_d^+ a_s^+/A^+$, where $y_d^+ = \sqrt{T^+/\pi}\ln(A^+/A_{th}^+)$ is the Stokes height (penetration depth) with a threshold amplitude $A^+_{\mathrm{th}} = 0.5$, and $a_s^+ = 2\pi A^+ \exp(-y^+\sqrt{\pi/T^+})/T^+$ is the maximum Stokes acceleration at a given y^+ (here $y^+ = 5$) [23,35]. The simulation results of SP flows from Fig. 2(c) are consistent with those of earlier research [8,21,22,33,36,37], and DR_o displays a linear correlation with S^+. The particle contribution DR_p exhibits an approximately exponential dependence on the dimensionless particle radius a^+, as shown in Fig. 2(d). As a^+ increases, the drag increase caused by the particles gradually weakens, and even a slight drag reduction can be achieved when the particles are large enough. The coupling term $\mathrm{DR}_{\mathrm{coup}}$ is modeled by

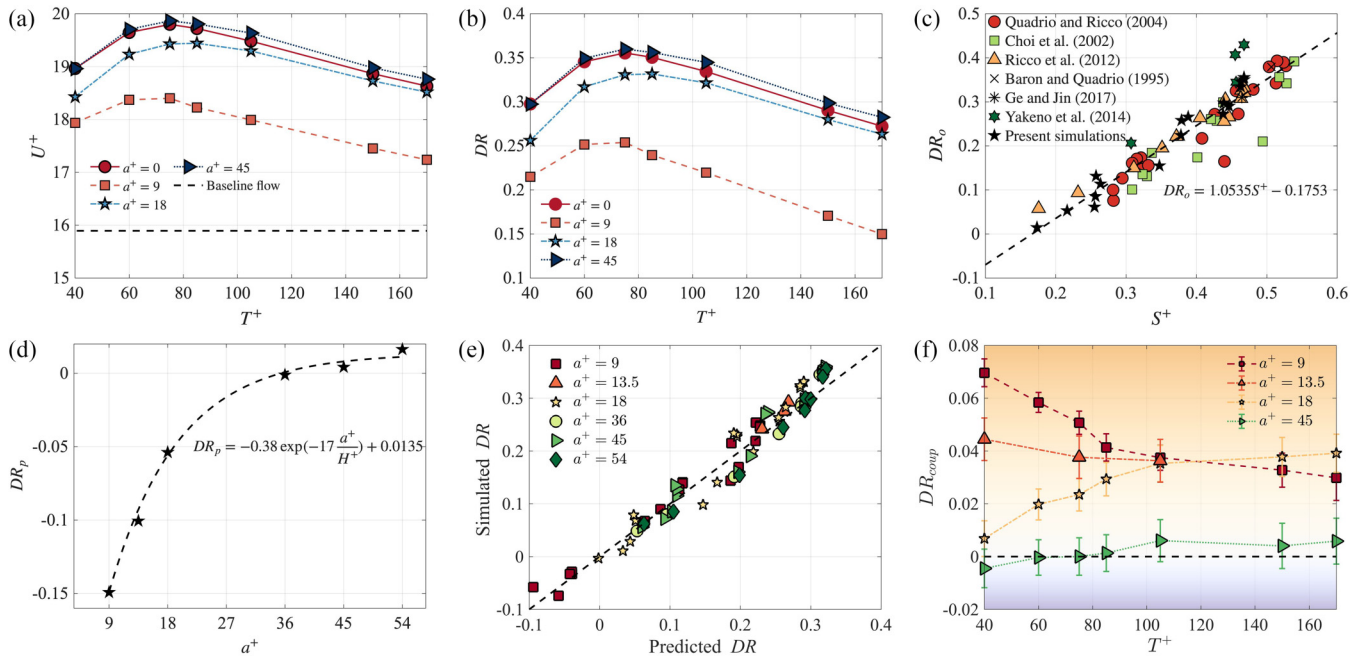


FIG. 2. (a) Temporal-spatial-averaged dimensionless velocities U^+ for the baseline and coupled conditions. (b) Drag reduction rate DR vs oscillation period under varying particle sizes. (c) Drag reduction rate from wall oscillation DR_o in the SP conditions. (d) Drag reduction rate from particles DR_p in the nonoscillatory conditions. (e) Comparison between simulated and predicted drag reduction rates. (f) Coupling effect $\mathrm{DR}_{\mathrm{coup}}$ [calculated using Eq. (7)] under different particle sizes and oscillation periods.

first- and second-order interaction terms of oscillation and particle contributions:

$$\mathrm{DR}_{\mathrm{coup}} \sim \mathrm{DR}_o\mathrm{DR}_p + \mathrm{DR}_o^2\mathrm{DR}_p + \mathrm{DR}_o\mathrm{DR}_p^2 + \mathrm{DR}_o^2\mathrm{DR}_p^2. \quad (8)$$

Figure 2(e) shows that the established model plays a good role ($R^2 = 0.98$) in accurately predicting drag reduction in the coupling flows, outperforming predictions that exclude the coupling term ($R^2 = 0.95$), thus highlighting the leading contribution of oscillation and the non-negligible role of the coupling regime.

Surprising to observe $\mathrm{DR}_{\mathrm{coup}} > 0$ in most cases in Fig. 2(f), indicating that the coupling between particles and span-wise wall oscillations consistently enhances drag reduction across a range of particle sizes. In other words, span-wise wall oscillations reduce drag more effectively in particle-laden flows than in single-phase flows. In essence, this enhancement is closely related to modifications in rheology and turbulent structures in the near-wall region.

The primary objective of drag reduction is to minimize energy consumption. To assess the energetic cost of the active control, we define the ratio of the power input for span-wise wall oscillations to that required for sustaining the stream-wise flow, denoted as P_{input} [38]. In the present configuration, P_{input} decreases with increasing oscillation period T^+, in agreement with previous studies [23,38]. The net energy saving is defined as $P_{\mathrm{net}} = P_{\mathrm{input}} + \mathrm{DR}$. Owing to the relatively large oscillation amplitude $A^+ = 12$, the overall P_{net} remains negative under the current conditions ($P_{\mathrm{net}} \in (-1, 0)$). Nevertheless, prior studies indicate that with appropriate tuning of oscillation parameters (e.g., reducing A^+), it is reasonable to expect positive net savings in PL flows, which will be further explored in future work.

The realization of drag reduction is intimately associated with the near-wall flow structures, particularly turbulent events in the boundary layer [39–41]. We assess the influence of oscillatory actuation through flow pattern visualization and quadrant analysis, as shown in Fig. 3. Stream-wise velocity u^+ rendered on the vortex structures demonstrates that the span-wise oscillations significantly increase u^+, improving flow discharge and achieving effective drag reduction in both SP and PL flows. The vortex structures identified using the Q criterion predominantly emerges around the high- and low-speed streaks, particularly in regions of intense shear where the high- and low-speed streaks are in close proximity. Compared to nonactuated flows, the reduction in density and stream-wise size of high- and low-speed streaks under oscillation is observed, implying a weakening of near-wall quasistreamwise vortices [42]. It suggests that the stream-wise and wall-normal velocity fluctuations near the wall are weakened, indicating a decrease in the momentum exchange between fluids at various normal heights and a thickening of the viscous sublayer [43]. It leads to a decrease in turbulent activity that partially accounts for drag reduction [22,23]. Span-wise oscillation modifies the critical ejection-sweep cycles in the near-wall region [44]. Quadrant analysis of DNS data in the viscous sublayer shows a significant reduction in the probability of sweep ($Q4$) events, $p(Q4)$, with a slight change in ejection ($Q2$) events, $p(Q2)$. In general, the probability of sweep events is inversely correlated with drag reduction [23]. In PL flows, wall oscillations reduce the combined ejection-sweep probability $p(Q2 + Q4)$ by 6.47% relative to the corresponding nonoscillatory PL flow, compared with a 5.92% reduction in SP flows relative to the nonoscillatory SP case. This stronger

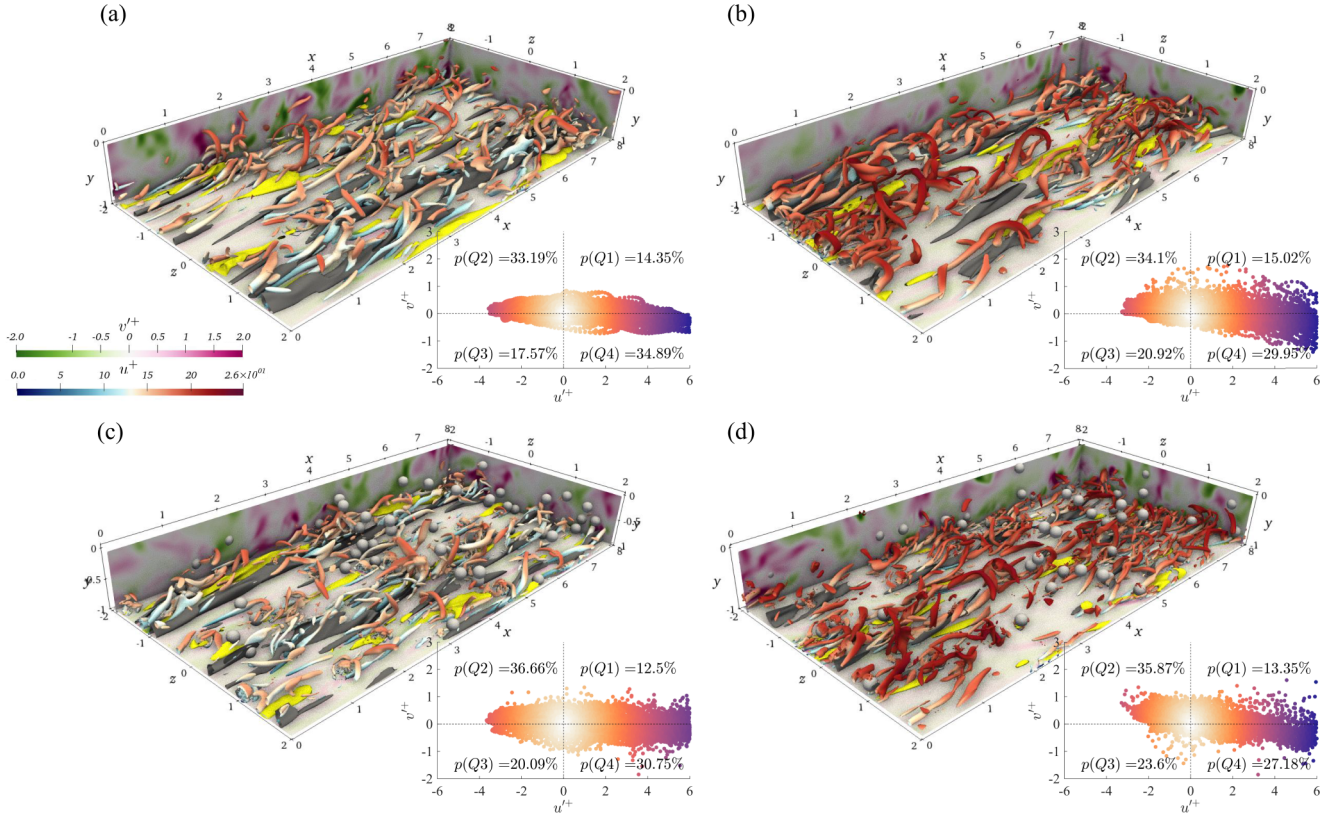


FIG. 3. Visualization of flow structures and quadrant analysis at (a) nonactuated SP flow, (b) actuated SP flow with $T^+ = 75$, (c) nonactuated PL flow, and (d) actuated PL flow with $T^+ = 75$. Vortical coherent structures extracted by the Q criterion ($Q^+ = 500$) are rendered by stream-wise fluid velocity u^+, ranging from blue (low) to red (high). High-speed streaks are depicted in yellow and low-speed streaks are shown in gray. The spatial distribution of wall-normal fluctuation velocity v'^+ is displayed in three slices. Insets present quadrant analysis at $y^+ = 5.63$ within the viscous sublayer.

suppression in PL flows explains the enhanced drag reduction ($\mathrm{DR}_{\mathrm{coup}} > 0$).

Viscosity is a key property for quantifying flow resistance [45–47]. In PL flows, the overall resistance is generally attributed to two major sources, including rheological contributions associated with particle-induced viscosity and stress variations (often parameterized by particle volume fraction), and fluid turbulence [5,30,48]. Among these, variations in near-wall viscosity play a particularly important role in explaining changes in flow drag. Against this broader background, the coupling drag reduction rate, $\mathrm{DR}_{\mathrm{coup}}$, is decomposed here into two components: a rheological contribution, $\mathrm{DR}^{\mathrm{rheo}}_{\mathrm{coup}}$, and a turbulence-dissipation contribution, $\mathrm{DR}^{\mathrm{turb}}_{\mathrm{coup}}$. These correspond to changes in rheological viscosity, ν^+_{rheo}, and turbulent viscosity, ν^+_{turb}, respectively, under spanwise wall oscillations in PL flows. The total effective viscosity is assumed by $\nu^+_{\mathrm{eff}} = \nu^+_{\mathrm{rheo}} + \nu^+_{\mathrm{turb}}$. To quantify near-wall dynamics, we define the integrated quantities $\Sigma_{(\cdot)}$ as

$$\Sigma_{(\cdot)} = \frac{1}{y^+_t}\int_0^{y^+_t} (\cdot) dy^+, \tag{9}$$

where $y^+_t = 7.5$ is the upper limit of integration (within the viscous sublayer). Depending on the integrand, this yields $\Sigma^{\mathrm{eff}}_\nu$, $\Sigma^{\mathrm{rheo}}_\nu$, $\Sigma^{\mathrm{turb}}_\nu$, and Σ_ϕ for ν^+_{eff}, ν^+_{rheo}, ν^+_{turb}, and ϕ, respectively. Notably, $\Sigma^{\mathrm{eff}}_\nu = \Sigma^{\mathrm{rheo}}_\nu + \Sigma^{\mathrm{turb}}_\nu$. In dilute granular flows, the rheological viscosity ν^+_{rheo} is approximated by the classical Einstein relation: $\nu^+_{\mathrm{rheo}}/\nu^+_0 \propto (1 + 2.5\phi)$ [49]. This model is used here to establish an approximate correlation between particle volume fraction and rheological viscosity. Such a simplified treatment is common in multiphase studies [50,51] and provides a practical closure, yielding the approximate linear relation $\Sigma^{\mathrm{rheo}}_\nu \sim \Sigma_\phi$.

For SP flows ($\Sigma_\phi = 0$ and $\Sigma^{\mathrm{rheo}}_\nu = \text{const.}$), the oscillation-induced drag reduction rate DR_o is modeled as a function of the difference in the cumulative near-wall viscosity due to oscillation, i.e., $\mathrm{DR}_o = f(\Sigma_{\nu,p} - \Sigma_{\nu,p+o})$. In PL flows, the turbulence-modulation component $\mathrm{DR}^{\mathrm{turb}}_{\mathrm{coup}}$ depends explicitly on the changes in turbulent viscosity, while $\mathrm{DR}^{\mathrm{rheo}}_{\mathrm{coup}}$ depends on changes in rheological viscosity and the particle size a^+. To characterize these effects, we define two key parameters: Δ_ϕ, proportional to the rheological viscosity variation ($\Delta_\phi \sim \Delta^{\mathrm{rheo}}_\nu$), and $\Delta^{\mathrm{turb}}_\nu$, expressed by

$$\Delta_\phi = a^+(\Sigma_{\phi,p} - \Sigma_{\phi,p+o}), \tag{10}$$

$$\Delta^{\mathrm{turb}}_\nu = \Sigma^{\mathrm{turb}}_{\nu,p} - \Sigma^{\mathrm{turb}}_{\nu,p+o}. \tag{11}$$

Here, the inclusion of the particle size a^+ ensures that Δ_ϕ accounts for the particle-size dependence. The apparent collapse of data across different particle diameters in Fig. 4(b) indicates that Δ_ϕ successfully captures the dominant contribution of

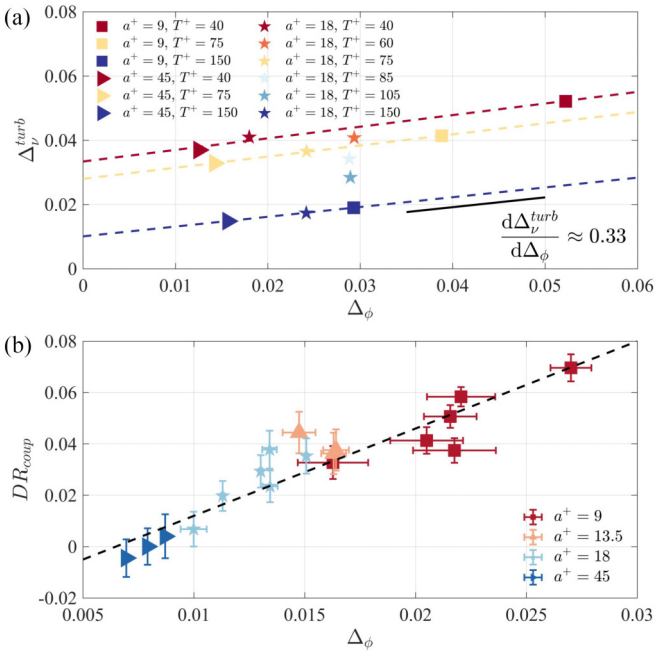


FIG. 4. (a) Near-wall integrated variation of turbulent viscosity Δ_ν^{turb} vs near-wall integrated variation of particle volume fraction Δ_ϕ. The dashed lines are the linear fitting results. (b) Relationship between the parameter Δ_ϕ and the coupling effect, DR_{coup}, in the rheology-based coupling effect prediction model. The black dashed line in panel (b) represents the result of a linear fit.

particle size together with local volume fraction variations within the present parameter regime. Figure 4(a) shows that Δ_ν^{turb} scales approximately linearly with Δ_ϕ for a fixed oscillation period T^+:

$$\Delta_\nu^{\text{turb}} = 0.33\Delta_\phi + c(T^+). \tag{12}$$

The fitted lines are drawn as indicative trends to highlight this monotonic systematic relationship. Equation (12) suggests that enhanced particle migration reduces near-wall turbulent viscosity. Assuming linear relationships between coupling component and viscosity variation, we express the coupling components ($\text{DR}_{\text{coup}}^{\text{rheo}}$ and $\text{DR}_{\text{coup}}^{\text{turb}}$) as

$$\text{DR}_{\text{coup}}^{\text{rheo}} \sim \Delta_\nu^{\text{rheo}} \sim \frac{2.5\nu_0^+}{a^+}\Delta_\phi, \quad \text{DR}_{\text{coup}}^{\text{turb}} \sim \Delta_\nu^{\text{turb}} \sim \Delta_\phi. \tag{13}$$

Hence, increased particle migration (Δ_ϕ) enhances both viscosities (Δ_ν^{rheo} and Δ_ν^{turb}), and demonstrates a linear dependence between Δ_ν^{rheo} and Δ_ν^{turb}. This coordination between Δ_ν^{rheo} and Δ_ν^{turb} effectively harmonizes the classical turbulent boundary layer theory and rheological theory explanations of flow drag. Additionally, $\text{DR}_{\text{coup}}^{\text{rheo}}$ is typically 3–4 orders of magnitude smaller than $\text{DR}_{\text{coup}}^{\text{turb}}$, highlighting that turbulence modulation dominates. Accordingly, the total coupling drag reduction rate can be approximated as

$$\text{DR}_{\text{coup}} = \text{DR}_{\text{coup}}^{\text{rheo}} + \text{DR}_{\text{coup}}^{\text{turb}} \sim \Delta_\phi. \tag{14}$$

with a functional fit observed in Fig. 4(b),

$$\text{DR}_{\text{coup}} = 3.4\Delta_\phi - 0.022. \tag{15}$$

This result supports the interpretation that span-wise wall oscillation enhances drag reduction by promoting particle migration toward the channel center—especially for small particles that exhibit stronger migration as shown in Fig. 1(c). Essentially, in wall-bounded turbulence, particles contribute to drag by disrupting coherent vortical structures (reflected in ν_{turb}^+) and by dissipating energy through fluid-particle forces (reflected in ν_{rheo}^+). Therefore, stronger migration (larger Δ_ϕ) leads to greater DR_{coup}, affirming the rheology-based predictive framework.

IV. CONCLUSIONS

In summary, this study uncovers a fundamental mechanism by which span-wise oscillatory forcing interacts with particle dynamics to achieve enhanced drag reduction in wall-bounded turbulent flows. Contrary to conventional expectations, we find that the presence of suspended particles strengthens the drag-reducing effect of wall oscillations. This counterintuitive result is traced to a positive coupling between particle-induced modulation of near-wall turbulence and the suppression of ejection-sweep cycles. Crucially, we demonstrate that the span-wise Stokes layer promotes particle migration away from the wall, reducing the near-wall particle volume fraction and, consequently, the effective viscosity. Based on the Einstein rheological model, we establish a quantitative relationship between the coupling drag reduction rate and a particle-rheology parameter that jointly accounts for the oscillation-driven variation in near-wall particle volume fraction and particle-size effect. This provides a rheological interpretation of the observed effects. Finally, by formulating a scaling law that links turbulent viscosity with rheological suspension viscosity, we reconcile classical turbulent boundary layer theory with rheological models, offering a cohesive framework for understanding particulate flow control.

These insights reveal general principles governing particle-turbulence-oscillation interactions, with implications extending beyond the present single-phase configuration. The work thus provides a physical paradigm for modulating multiphase turbulence and contributes broadly to the fundamental understanding of drag-reduction physics in complex fluids.

ACKNOWLEDGMENTS

This research was supported by National Natural Science Foundations of China under Grants No. 12222211 and No. 91852205, and Zhejiang Provincial Natural Science Foundation of China under Grant No. LZ25A020005.

DATA AVAILABILITY

The data supporting this study's findings are available within the article.

[1] X. Ting, Z. Xinzhuo, S. A. Miedema, and C. Xiuhan, Study of the characteristics of the flow regimes and dynamics of coarse particles in pipeline transportation, Powder Technol. **347**, 148 (2019).
[2] S. L. Sinha, S. K. Dewangan, and A. Sharma, A review on particulate slurry erosive wear of industrial materials: In context with pipeline transportation of mineral-slurry, Part. Sci. Technol. **35**, 103 (2017).
[3] J. Grace and G. Sun, Influence of particle size distribution on the performance of fluidized bed reactors, Can. J. Chem. Eng. **69**, 1126 (1991).
[4] B. Y. Shekunov, P. Chattopadhyay, H. H. Tong, and A. H. Chow, Particle size analysis in pharmaceutics: Principles, methods and applications, Pharm. Res. **24**, 203 (2007).
[5] L. Brandt and F. Coletti, Particle-laden turbulence: Progress and perspectives, Annu. Rev. Fluid Mech. **54**, 159 (2022).
[6] S. Balachandar and J. K. Eaton, Turbulent dispersed multiphase flow, Annu. Rev. Fluid Mech. **42**, 111 (2010).
[7] W.-J. Jung, N. Mangiavacchi, and R. Akhavan, Suppression of turbulence in wall-bounded flows by high-frequency spanwise oscillations, Phys. Fluids **4**, 1605 (1992).
[8] M. Quadrio and P. Ricco, Critical assessment of turbulent drag reduction through spanwise wall oscillations, J. Fluid Mech. **521**, 251 (2004).
[9] Y. Du and G. E. Karniadakis, Suppressing wall turbulence by means of a transverse traveling wave, Science **288**, 1230 (2000).
[10] I. Marusic, D. Chandran, A. Rouhi, M. K. Fu, D. Wine, B. Holloway, D. Chung, and A. J. Smits, An energy-efficient pathway to turbulent drag reduction, Nat. Commun. **12**, 5805 (2021).
[11] M. Quadrio, P. Ricco, and C. Viotti, Streamwise-travelling waves of spanwise wall velocity for turbulent drag reduction, J. Fluid Mech. **627**, 161 (2009).
[12] F. Auteri, A. Baron, M. Belan, G. Campanardi, and M. Quadrio, Experimental assessment of drag reduction by traveling waves in a turbulent pipe flow, Phys. Fluids **22**, 115103 (2010).
[13] K. Fukagata, K. Iwamoto, and Y. Hasegawa, Turbulent drag reduction by streamwise traveling waves of wall-normal forcing, Annu. Rev. Fluid Mech. **56**, 69 (2024).
[14] D. Bechert, M. Bruse, W. V. Hage, J. T. Van der Hoeven, and G. Hoppe, Experiments on drag-reducing surfaces and their optimization with an adjustable geometry, J. Fluid Mech. **338**, 59 (1997).
[15] R. García-Mayoral and J. Jiménez, Drag reduction by riblets, Philos. Trans. R. Soc. A **369**, 1412 (2011).
[16] J. M. J. Toonder, F. Nieuwstadt, and G. Kuiken, The role of elongational viscosity in the mechanism of drag reduction by polymer additives, Appl. Sci. Res. **54**, 95 (1995).
[17] V. S. L'vov, A. Pomyalov, I. Procaccia, and V. Tiberkevich, Drag reduction by polymers in wall bounded turbulence, Phys. Rev. Lett. **92**, 244503 (2004).
[18] C. M. White and M. G. Mungal, Mechanics and prediction of turbulent drag reduction with polymer additives, Annu. Rev. Fluid Mech. **40**, 235 (2008).
[19] G. H. Choueiri, J. M. Lopez, and B. Hof, Exceeding the asymptotic limit of polymer drag reduction, Phys. Rev. Lett. **120**, 124501 (2018).
[20] E. Touber and M. A. Leschziner, Near-wall streak modification by spanwise oscillatory wall motion and drag-reduction mechanisms, J. Fluid Mech. **693**, 150 (2012).
[21] A. Baron and M. Quadrio, Turbulent drag reduction by spanwise wall oscillations, Appl. Sci. Res. **55**, 311 (1996).
[22] P. Ricco, C. Ottonelli, Y. Hasegawa, and M. Quadrio, Changes in turbulent dissipation in a channel flow with oscillating walls, J. Fluid Mech. **700**, 77 (2012).
[23] P. Ricco, M. Skote, and M. A. Leschziner, A review of turbulent skin-friction drag reduction by near-wall transverse forcing, Prog. Aerosp. Sci. **123**, 100713 (2021).
[24] R. Glowinski, T.-W. Pan, T. I. Hesla, and D. D. Joseph, A distributed Lagrange multiplier/fictitious domain method for particulate flows, Int. J. Multiphase Flow **25**, 755 (1999).
[25] Z. Yu and X. Shao, A direct-forcing fictitious domain method for particulate flows, J. Comput. Phys. **227**, 292 (2007).
[26] C. Zhu, Z. Yu, X. Shao, and J. Deng, Interface-resolved numerical simulations of particle-laden turbulent flows in a vertical channel filled with Bingham fluids, J. Fluid Mech. **883**, A43 (2020).
[27] Y. Xia, H. Xiong, Z. Yu, and C. Zhu, Effects of the collision model in interface-resolved simulations of particle-laden turbulent channel flows, Phys. Fluids **32**, 103303 (2020).
[28] P. G. Saffman, The lift on a small sphere in a slow shear flow, J. Fluid Mech. **22**, 385 (1965).
[29] X. Shao, Z. Yu, and B. Sun, Inertial migration of spherical particles in circular Poiseuille flow at moderately high Reynolds numbers, Phys. Fluids **20**, 103307 (2008).
[30] F. Picano, W.-P. Breugem, and L. Brandt, Turbulent channel flow of dense suspensions of neutrally buoyant spheres, J. Fluid Mech. **764**, 463 (2015).
[31] P. Costa, F. Picano, L. Brandt, and W.-P. Breugem, Universal scaling laws for dense particle suspensions in turbulent wall-bounded flows, Phys. Rev. Lett. **117**, 134501 (2016).
[32] X. Shao, T. Wu, and Z. Yu, Fully resolved numerical simulation of particle-laden turbulent flow in a horizontal channel at a low Reynolds number, J. Fluid Mech. **693**, 319 (2012).
[33] J.-I. Choi, C.-X. Xu, and H. J. Sung, Drag reduction by spanwise wall oscillation in wall-bounded turbulent flows, AIAA J. **40**, 842 (2002).
[34] Z. Li, S. Ji, H. Duan, S. Lan, J. Zhang, and P. Lv, Coupling effect of wall slip and spanwise oscillation on drag reduction in turbulent channel flow, Phys. Rev. Fluids **5**, 124601 (2020).
[35] D. J. Wise and P. Ricco, Turbulent drag reduction through oscillating discs, J. Fluid Mech. **746**, 536 (2014).
[36] M. Ge and G. Jin, Response of turbulent enstrophy to sudden implementation of spanwise wall oscillation in channel flow, Appl. Math. Mech. **38**, 1159 (2017).
[37] A. Yakeno, Y. Hasegawa, and N. Kasagi, Modification of quasi-streamwise vortical structure in a drag-reduced turbulent channel flow with spanwise wall oscillation, Phys. Fluids **26**, 085109 (2014).
[38] C. Viotti, M. Quadrio, and P. Luchini, Streamwise oscillation of spanwise velocity at the wall of a channel for turbulent drag reduction, Phys. Fluids **21**, 115109 (2009).
[39] C. White, V. Somandepalli, and M. Mungal, The turbulence structure of drag-reduced boundary layer flow, Exp. Fluids **36**, 62 (2004).
[40] E. Aljallis, M. A. Sarshar, R. Datla, V. Sikka, A. Jones, and C.-H. Choi, Experimental study of skin friction drag reduction on superhydrophobic flat plates in high Reynolds number boundary layer flow, Phys. Fluids **25**, 025103 (2013).

[41] H. Choi, P. Moin, and J. Kim, Active turbulence control for drag reduction in wall-bounded flows, J. Fluid Mech. **262**, 75 (1994).
[42] I. Marusic, R. Mathis, and N. Hutchins, Predictive model for wall-bounded turbulent flow, Science **329**, 193 (2010).
[43] K.-S. Choi, J.-R. DeBisschop, and B. R. Clayton, Turbulent boundary-layer control by means of spanwise-wall oscillation, AIAA J. **36**, 1157 (1998).
[44] A. Ferrante and S. Elghobashi, On the physical mechanisms of drag reduction in a spatially developing turbulent boundary layer laden with microbubbles, J. Fluid Mech. **503**, 345 (2004).
[45] P. Costa, F. Picano, L. Brandt, and W.-P. Breugem, Effects of the finite particle size in turbulent wall-bounded flows of dense suspensions, J. Fluid Mech. **843**, 450 (2018).
[46] N. Phan-Thien and J. Dudek, Pulsating flow of a plastic fluid, Nature (London) **296**, 843 (1982).
[47] Y. Lin, G. W. H. Tan, N. Phan-Thien, and B. C. Khoo, Flow enhancement in pulsating flow of non-colloidal suspensions in tubes, J. Non-Newtonian Fluid Mech. **212**, 13 (2014).
[48] Q. Zhang and A. Prosperetti, Physics-based analysis of the hydrodynamic stress in a fluid-particle system, Phys. Fluids **22**, 033306 (2010).
[49] A. Einstein, Eine neue Bestimmung der Moleküldimensionen, Ph.D. thesis, ETH Zurich, 1905.
[50] M. Eesa and M. Barigou, Horizontal laminar flow of coarse nearly-neutrally buoyant particles in non-Newtonian conveying fluids: CFD and PEPT experiments compared, Int. J. Multiphase Flow **34**, 997 (2008).
[51] E. Montellà, J. Chauchat, B. Chareyre, C. Bonamy, and T. Hsu, A two-fluid model for immersed granular avalanches with dilatancy effects, J. Fluid Mech. **925**, A13 (2021).